Synthesis, Structural Analysis, and Superconductivity of $Ba_xV_6S_8$

Omar Fuentes,[†] Hsien-Hau Wang,[‡] Brian H. Ward,[‡] Jianhua Zhang,[†] Davide M. Proserpio,[§] Frank Calvagna,[†] Catherine E. Check,[†] Kim C. Lobring,[†] and Chong Zheng*[,†]

Department of Chemistry and Biochemistry, Northern Illinois University, DeKalb, Illinois 60115, Materials Science Division, Argonne National Laboratory, Argonne, Illinois 60439, and Dipartimento di Chimica Strutturale e Stereochimica Inorganica, Università di Milano, I-20133 Milano, Italy

Received May 15, 2000. Revised Manuscript Received June 21, 2001

A nonstoichiometric ternary vanadium sulfide, $Ba_xV_6S_8$ ($x = 0.41-0.48$), was synthesized. This solid-state compound crystallizes in the hexagonal space group $P6_3/m$ (no. 176) with $a = 9.2080(3)$ Å, $c = 3.3169(2)$ Å, $V = 243.55(2)$ Å^3, and $Z = 1$. The structure of this solid is similar to that of its parent compound V_3S_4, consisting of face-sharing, distorted octahedral VS_6 units. A superconducting transition of the solid at approximately 2.5 K was observed. A computational analysis of the electronic structure using the extended Hückel method is presented.

Introduction

Superconducting transitions are well-known for the Chevrel phases $M_xMo_6S_8$ and $M_xMo_6Se_8$, where M is a dopant metal such as Pb, In, Tl, or La.[1,2] Not many ternary group 5 transition metal chalcogenides of similar composition, however, are known to be superconductors. The Nb_3S_4 and isostructural V_3S_4 phases present good candidates for superconductivity as the large channels parallel to the *c* axis can accommodate a variety of ions, allowing for the fine-tuning of the electronic configuration of the structure.[3−6] Recently, superconductivity of the Tl- and In-doped vanadium sulfides $Tl_xV_6S_8$ and $In_xV_6S_8$ ($x = 0.03-0.78$) was reported for the first time by Bensch and co-workers.[4,7] The superconducting transition temperature T_c ranges from 3.7 to 4.8 K. Alkali-metal- and silver-doped compounds such as $K_xV_6S_8$ and $Ag_xV_6S_8$, nevertheless, did not exhibit superconductivity.[8] On the other hand, many Ba-containing vanadium sulfides have been synthesized. Examples include $BaVS_3$,[9−13] $Ba_{0.5}V_5S_8$,[14] and $BaVS_{2.955}$.[15] None of these compounds has been reported to exhibit superconducting properties.[16] In our own measurements, we did not observe a superconducting transition for $BaVS_3$ above 2 K. This leads to speculation that a group 13 dopant element is required for the occurrence of superconductivity. In this contribution, we report the synthesis and observation of a superconducting transition for the Ba-doped compound $Ba_xV_6S_8$ ($x = 0.41-0.48$). The electronic structure is also analyzed using the tight-binding extended Hückel method.[17,18]

Experimental Section

The synthesis of $Ba_xV_6S_8$ was carried out using the flux growth method. KCl powder was used as the flux and was previously dried at 250 °C under a vacuum over a period of 48 h. The synthesis was initiated by placing powdery BaS, V, and S in a quartz ampule in the molar ratio of 1:1:0.55. The total weight of the sample was approximately 0.5 g. Two grams of KCl flux was added to and mixed with the sample. The quartz ampule containing the sample and flux was evacuated to about 10^{-4} Torr and sealed. A computer-controlled furnace was used to heat the ampule from room temperature to 400 °C in 12 h to allow the sulfur component to react first, and the temperature was increased subsequently from 400 to 900 °C in 12 h. The reaction temperature was held at 900 °C for 72 h. The ampule was then cooled from 900 to 600 °C in 36 h and then from 600 °C to room temperature in 12 h. Needlelike

* Author to whom correspondence should be addressed: Dr. Chong Zheng, Department of Chemistry, Northern Illinois University, DeKalb, IL 60115. Telephone: (815) 753-6871. Fax: (815) 753-4802. E-mail:zheng@cz.chem.niu.edu.

[†] Northern Illinois University.

[‡] Argonne National Laboratory.

[§] Università di Milano.

(1) Tarascon, J. M.; DiSalvo, F. J.; Murphy, D. W.; Hull, G.; Waszczak, J. V. *Phys. Rev. B* **1984**, *29*, 172.

(2) Peña, O.; Le Berre, F.; Hamard, C.; Corrignan, A.; Horyn, R.; Wjakowski, A. *J. Alloys Compd.* **1997**, *262−263*, 331.

(3) Bensch, W.; Koy, J. *Acta Crystallogr. C* **1993**, *49*, 1133.

(4) Bensch, W.; Koy, J.; Biberacher, W. *Mater. Res. Bull.* **1995**, *30*, 1217.

(5) Boswell, F. W.; Bennett, J. C.; Prodan, A. *J. Solid State Chem.y* **1999**, *144*, 454.

(6) Bensch, W.; Schnieder, M.; Muhler, M.; Biberacher, W.; Knecht, M.; Vernes, A.; Ebert, H. *J. Alloys Compd.* **1996**, *244*, 59.

(7) Bensch, W.; Koy, J.; Biberacher, W. *Solid State Commun.* **1995**, *93*, 261.

(8) Bronsema, K. D.; Wiegers, G. A. *Mater. Res. Bull.* **1987**, *22*, 1073.

(9) Marezio, M. *Chem. Scr.* **1986**, *26*, 91.

(10) Kelber, J.; Jorgensen, J. D.; Mueller, M. H. *Acta Crystallogr.* **1979**, *35*, 2473.

(11) Ghedira, M.; Anne, M.; Chenavas, J.; Marezio, M.; Sayetat, F. *J. Phys. C* **1986**, *19*, 6489.

(12) Ghedira, M.; Chenavas, J.; Sayetat, F.; Marezio, M.; Massenet, O.; Mercier, J. *Acta Crystallogr. B* **1981**, *37*, 1491.

(13) Gardner, R. A.; Vlasse, M.; Wold, A. *Acta Crystallogr. B* **1969**, *25*, 781.

(14) Petricek, S.; Boller, H.; Klepp, K. O. *Solid State Ionics* **1995**, *81*, 183.

(15) Poulsen, N. J. *Mater. Res. Bull.* **1997**, *32*, 1673.

(16) Nagata, S.; Atake, T. *J. Therm. Anal. Calorim.* **1999**, *57*, 807.

(17) Whangbo, M. H.; Hoffmann, R.; Woodward, R. B. *Proc. R. Soc. London* **1979**, *A366*, 23.

(18) Hoffmann, R. *J. Chem. Phys.* **1963**, *39*, 1397.

10.1021/cm000396d CCC: $20.00
Published on Web 09/17/2001

Table 1. Crystal Data and Structure Refinement for $Ba_xV_6S_8$

empirical formula	$Ba_xS_8V_6$	
formula weight	699.46	
temperature	293(2) K	
wavelength	0.71073 Å	
crystal system	hexagonal	
space group	$P6_3/m$	
unit cell dimensions	$a = 9.2080(3)$ Å	$\alpha = 90°$
	$b = 9.2080(3)$ Å	$\beta = 90°$
	$c = 3.3169(2)$ Å	$\gamma = 120°$
volume	243.553(18) Å^3	
Z	1	
density (calculated)	4.769 Mg/m^3	
absorption coefficient	11.129 mm^{-1}	
$F(000)$	322	
θ range for data collection	2.55−27.73°	
index ranges	$-7 \le h \le 11$, $-12 \le k \le 10$, $-4 \le l \le 4$	
reflections collected	1589	
independent reflections	227 [R(int) = 0.0286]	
completeness to $\theta = 27.73°$	99.6%	
absorption correction	semiempirical from equivalents	
max and min transmission	1.000 and 0.733955	
refinement method	full-matrix least-squares on F^2	
data/restraints/parameters	227/0/19	
goodness-of-fit on F^2	1.374	
final R indices[a] [$I > 2\sigma(I)$]	R1 = 0.0240, wR2 = 0.0560	
R indices[a] (all data)	R1 = 0.0258, wR2 = 0.0567	
largest diff peak and hole	0.625 and −0.548 e Å^{-3}	

[a] $R1 = \sum||F_o| - |F_c||/\sum|F_o|$; $wR2 = [\sum[w(F_o^2 - F_c^2)^2]/\sum[w(F_o^2)^2]]^{1/2}$.

Table 2. Atomic Coordinates (× 10^4) and Equivalent Isotropic Displacement Parameters (Å^2 × 10^3) for $Ba_xV_6S_8$

atom	Wyckoff Site	x	y	z	U(eq)[a]
V	6h	4888(1)	1196(1)	2500	8(1)
S(1)	6h	3477(1)	2968(1)	2500	8(1)
S(2)	2d	3333	6667	2500	7(1)
Ba	2a	0	0	2500	68(1)

[a] U(eq) is defined as one-third of the trace of the orthogonalized U^{ij} tensor

crystals were formed in the KCl flux. The KCl flux was then washed from the sample with distilled water.

Several crystals of the compound were indexed on a Siemens SMART CCD diffractometer using 40 frames with an exposure time of 20 s per frame. All exhibited the same hexagonal cell. Ten of these crystals were used for data collection. All data sets confirmed similar amounts of doping of Ba ($x = 0.41-0.48$), but only one typical data set is reported here. A total of 1589 reflections were collected in the hemisphere of the reciprocal lattice of the hexagonal cell, of which 227 were unique with R(int) = 0.0286. An empirical absorption correction using the program SADABS[19] was applied to all observed reflections. The structure was solved with the direct method using the SHELXS and SIR97 programs;[19,20] both programs yielded the same structure. Full-matrix least-squares refinement on F^2 was carried out using the SHELXL-97 program.[19] The final agreement factor values are R1 = 0.0240, wR2 = 0.0560 ($I > 2\sigma$). The final structure was checked for additional symmetry with the MISSYM algorithm[21] implemented in the PLATON program suite.[22] No additional symmetry was found. The unit cell information and refinement details are reported in Table 1. The atomic positions and equivalent isotropic displacement parameters are listed in Table 2. Selected bond lengths and angles are presented in Table 3.

EDAX analysis using the microprobe of a JEOL 35 CF−Kevex μx 7000 scanning electron microscope confirmed the presence of Ba, V, and S in the same crystals used for X-ray data collection. The elemental ratio also agreed with that determined by the X-ray measurement.

Table 3. Bond Lengths (Å) and Angles (degrees) for $Ba_xV_6S_8$[a]

V−S(1)#1 (X 2)	2.3555(11)
V−S(1)#2 (X 4)	2.3588(8)
V−S(2)#4 (X 8)	2.4665(5)
V−S(2)#5	2.4665(5)
V−S(1)	2.5436(10)
V−V#6 (X 2)	2.8459(10)
S(1)−Ba (X 3)	2.9948(9)
S(1)−Ba#11 (X 7)	3.4233(8)
S(1)#1−V−S(1)#2 (X 2)	105.73(3)
S(1)#2−V−S(1)#3	89.35(4)
S(1)#1−V−S(2)#4 (X 2)	84.42(2)
S(1)#2−V−S(2)#4 (X 2)	168.95(3)
S(1)#3−V−S(2)#4 (X 2)	92.063(16)
S(2)#4−V−S(2)#5	84.502(19)
S(1)#1−V−S(1)	159.70(4)
S(1)#2−V−S(1) (X 2)	88.50(4)
S(2)#4−V−S(1) (X 2)	80.59(2)

[a] Symmetry transformations used to generate equivalent atoms: #1 $-y + 1, x - y, z$; #2 $y, -x + y, -z$; #3 $y, -x + y, -z + 1$; #4 $-x + 1, -y + 1, -z + 1$; #5 $-x + 1, -y + 1, -z$; #6 $-x + 1, -y, -z$; #7 $-x + 1, -y, -z + 1$; #8 $-x + y + 1, -x + 1, z$; #9 $x - y, x, -z + 1$; #10 $x - y, x, -z$; #11 $-x, -y, -z$; #12 $-x, -y, -z + 1$; #13 $y, -x + y + 1, -z$; #14 $y, -x + y + 1, -z + 1$; #15 $-x + y, -x, z$; #16 $-y, x - y, z$; #17 $x, y, z + 1$; #18 $x, y, z - 1$.

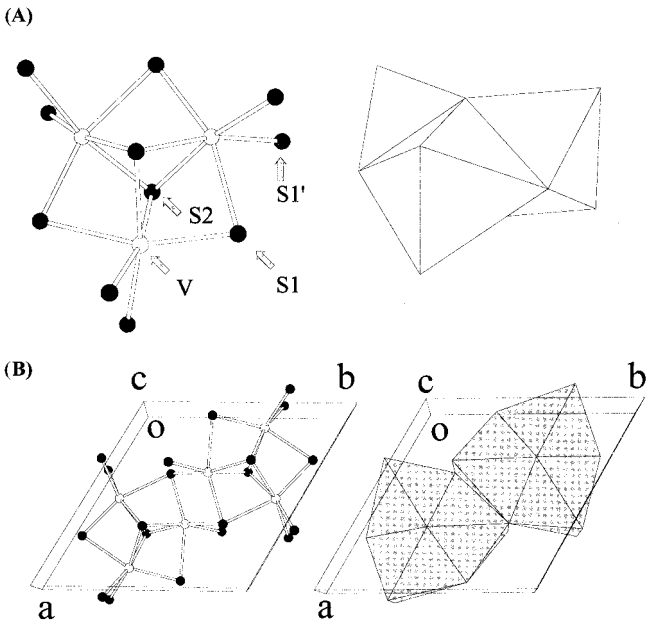

Figure 1. (A) Basic building unit of $Ba_xV_6S_8$. It consists of three distorted face-sharing octahedra. The left side is a top view showing the coordination geometry, and the right panel is a side view of the packing of the three octahedra. (B) Unit cell contains two face-sharing octahedron trimers. They are joined together by sharing an octahedron edge. The left side is a top view showing the coordination environment, and the right side is a view of the packing of the six octahedra.

The AC magnetic susceptibility of the sample (16.982 mg) in the temperature range from 300 to 1.2 K was measured using a LakeShore 7000 ac susceptometer. The AC modulation frequency used was 125 Hz, and the AC field was 1 G. The sample was cooled from room temperature to 4 K over a period of 15 min and then further cooled to 1.2 K.

Raman spectra were recorded with a Raman microscope spectrometer (Renishaw Ltd.) equipped with a He−Ne (λ_0 = 6328 Å) laser. Low laser power of ca. 0.06 mW focused on a 1 μm^2 area was applied. The spectra were averaged over 10 or more runs.

(19) Sheldrick, G. M. *SHELXTL*, version 5; Siemens Analytical Instruments Inc.: Madison, WI, 1994.
(20) Altomare, A.; Cascarano, G.; Giacovazzo, C.; Guagliardi, A.; Burla, M. C.; Polidori, G.; Camalli, M. *J. Appl. Crystallogr.* **1994**, *27*, 435.
(21) Le Page, Y. *J. Appl. Crystallogr.* **1987**, *20*, 264.
(22) Spek, A. L. *Acta Crystallogr. A: Found. Crystallogr.* **1990**, *46*, C34.

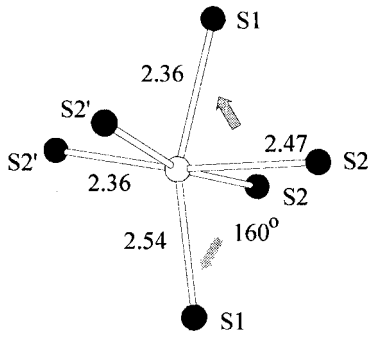

1

Results and Discussion

Structure. The basic unit of the structure is a face-sharing octahedron trimer, as shown in Figure 1A. Three sulfur atoms (S1 in Figure 1B) form the corner of a triangle, and three vanadium atoms are at the edges of the triangle. Another sulfur atom (S2) is at the center of the triangle. Figure 1A shows two such atoms, but they are related by a translation along the *c* axis. Each vanadium atom is coordinated to six sulfur atoms.

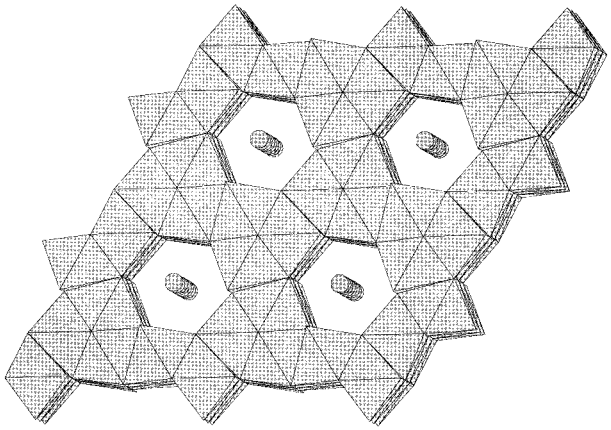

Figure 2. Face-sharing octahedron trimers joined with those in adjacent cells and stacked along the *c* axis. Hexagonal channels are formed. The diameter of the channels is approximately 6.2 Å. Ba atoms form columns in the channels.

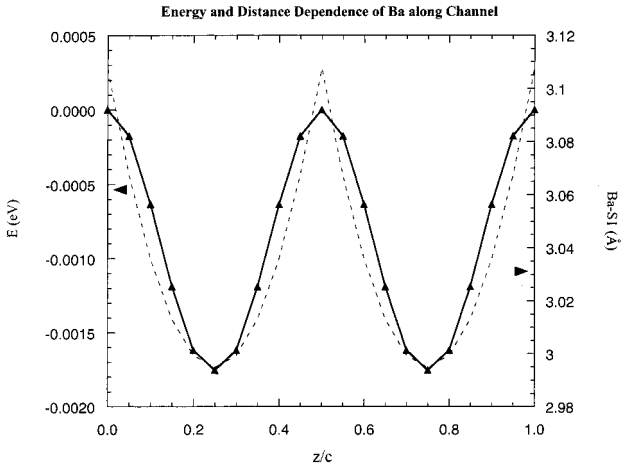

Figure 3. Relative energy (left *y* axis) and Ba−S1 distance (right *y* axis) as a function of the *z*/*c* coordinate of the Ba atom in the channel parallel to the *c* axis. $Z/c = {}^1/_4$ corresponds to the Wyckoff position 2a.

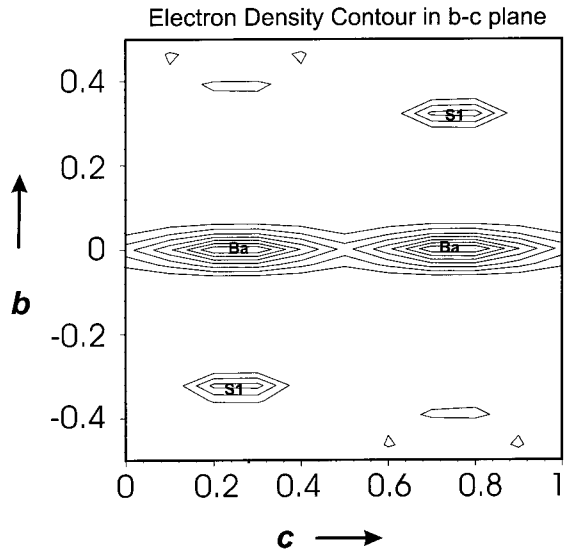

Figure 4. Electron density plot at the *bc* plane ($x/a = 0$) showing the elongated ellipsoid along the *c* axis for the Ba atoms.

Table 4. Extended Hückel Parameters

	orbital	H_{ii} (eV)	$\zeta_1{}^a$	ζ_2	$c_1{}^a$	c_2
Ba	6s	−7.0	2.2			
	6p	−4.0	2.2			
V	4s	−8.81	1.3			
	4p	−5.52	1.3			
	3d	−11.00	4.75	1.7	0.4755	0.7052
S	3s	−20.0	1.817			
	3p	−13.3	1.817			

[a] Exponents and coefficients in a double ζ expansion of the d orbital.

Among the six sulfur atoms, two are at the corner of the triangle (S1), two are at the center of the triangle shared with another unit cell (S2), and the remaining two are on the outside of the triangle (S1′). These S1′ atoms belong to another octahedron trimer. Thus, there are total of three vanadium atoms, three type-S1 sulfur atoms, and one type-S2 sulfur atom, giving a stoichiometric ratio of V_3S_4 per such a trimeric unit.

In order for the three octahedra to share faces in this trimeric unit, a distortion must occur. **1** shows the local coordination environment of the vanadium atom. As can be seen, the most visible distortion is the bending of the S1−V−S1 angle from 180° to 159.8° (only three significant figures are shown in **1** for clarity). One of the apical V−S1 bonds is shorter (2.355 Å) than the other (2.544 Å), compared to the basal V−S2 bonds of 2.467 and 2.359 Å. The other four basal S2−V−S2 angles also distort from the ideal 90° to 84.5°, 92.1°, 92.1° and 89.3°, respectively.

In the unit cell, there are two such octahedron trimers, as shown in Figure 1B. They are joined together by sharing an octahedron edge. These units are stacked along the *c* axis, again by sharing the octahedron edges, as shown in Figure 2. It is interesting to note that channels are formed along the *c* axis as a result of the octahedron stacking. The size of the channels is rather large, with a diameter of about 6.2 Å. The dopant Ba atoms form columns in the channels. However, the sites (Wyckoff symmetry 2a) are not fully occupied despite the large void in the channel. About 22% of the 2a sites are statistically occupied. The large channel allows the

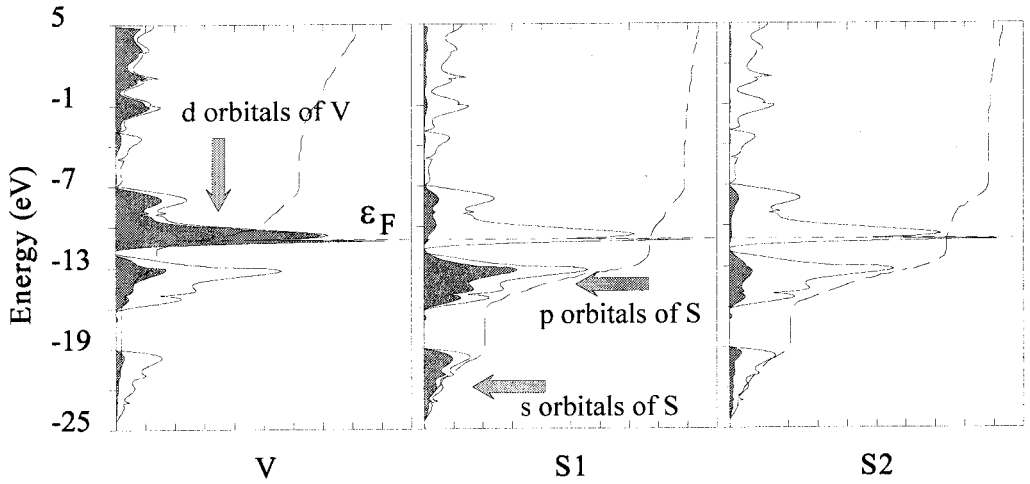

Figure 5. Computed DOS of $Ba_xV_6S_8$. The shaded area is the projected DOS, the solid curve is the total DOS, and the dashed curve is the integrated DOS. The left panel shows the projected V states, the middle panel shows the projected states of type-S1 sulfur atoms, and the right panel shows the projected DOS of type-S2 sulfur atoms.

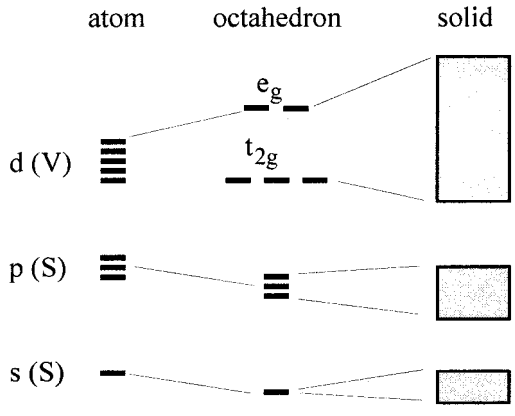

2

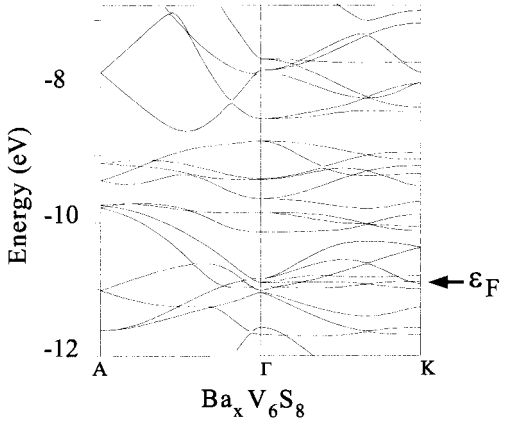

Figure 6. Computed band structure of $Ba_xV_6S_8$. Only the d band region is shown. The special points in the Brillouin zone are A(0,0,$^1/_2$), Γ(0,0,0), and K($^1/_2$,$^1/_2$,0).

dopant Ba atoms to move without a large energy cost. Figure 3 shows the energy dependence of a Ba atom moving along the channel as calculated by the extended Hückel method.[17,18] The 2a position ($z = {}^1/_4$) is the local energy minimum. This is because, at this position, Ba^{2+} ion has the closest contact with the sulfur anion (S1) at 2.9948 Å. In Figure 3, the relative energy (left *y* axis) follows exactly the same trend as the Ba−S1 distance (right *y* axis). Because of the low energy barrier, the thermal parameter of Ba along the *c* axis (U_{33}) is rather large, as shown in the electron density contour plot in Figure 4. This type of thermal ellipsoid elongation has been observed in other channel structures.[23]

If the 2a sites were 100% occupied, the stoichiometric ratio would be $Ba_2V_6S_8$. With this stoichiometry, it is likely that there would be too many valence electrons for this compound. To understand this aspect, we analyzed the electronic structure of this compound using the tight-binding extended Hückel method.[17,18] The parameters used in the computation are listed in Table 4. The density of states (DOS) and crystal orbital overlap population (COOP)[24] were computed using a set of 125 *k* points in the irreducible wedge of the Brillouin zone.

Computational Analysis. The electronic structure of the compound can be understood by a stepwise construction of interaction diagrams. In an S_6 octahedron, the d orbitals of the vanadium atoms split into a lower t_{2g} set and a higher e_g set. When the octahedra share edges, the vanadium−vanadium distance between the trimers is short at 2.8459 Å. Thus, we expect these two sets develop into bands along the *a* and *b* axes where the edge-sharing octahedra propagate. This is shown schematically in **2**. Figure 5 shows the computed DOS. Indeed, the sulfur s and p orbitals are at the lower part of the plot at around −20 eV and −13 eV, respectively. The vanadium d state is at around −10 eV. Along the *c* axis, the octahedra share other edges, and the shortest vanadium−vanadium bond (2.8459 Å) propagates in a zigzag fashion parallel to the *c* axis. Thus, we expect the band dispersion to be larger along the *c* axis than along the *a* and *b* axes. Figure 6 shows the computed band structure in the vanadium d band region. It can be seen in this figure that the band dispersion is larger along the A(0,0,$^1/_2$)−Γ line (parallel to the *c* axis) than along the Γ−K($^1/_2$,$^1/_2$,0) line (perpendicular to the *c* axis).

(23) Wörle, M.; Nesper, R. *Angew. Chem.* **2000**, *112*, 2439.

(24) Wijeyesekera, S. D.; Hoffmann, R. *Organometallics* **1984**, *3*, 949.

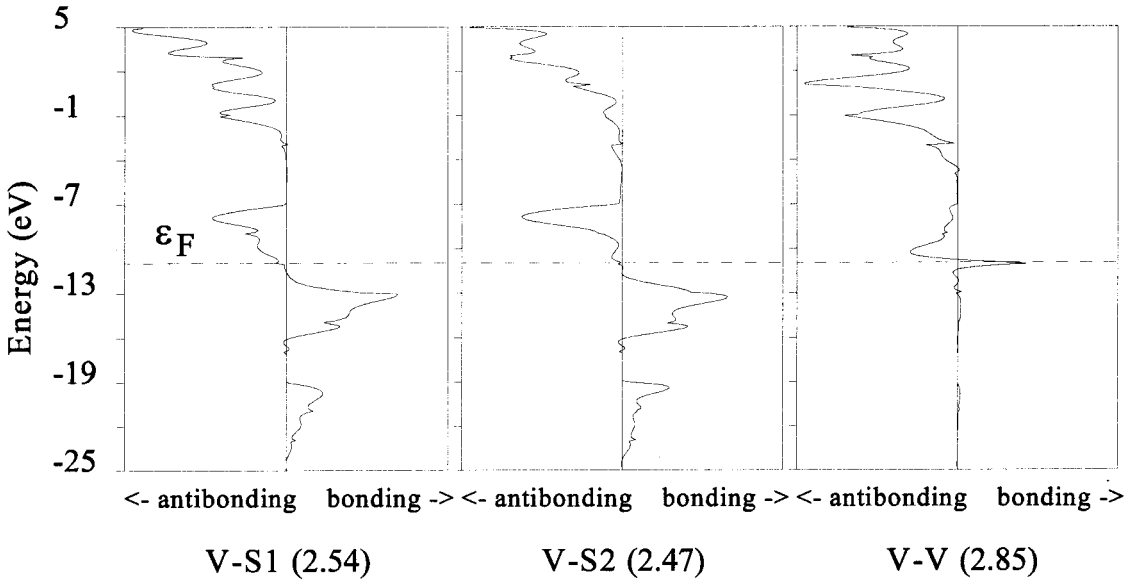

Figure 7. Computed COOP curves of various bonds in $Ba_xV_6S_8$. The bond distances are in parentheses.

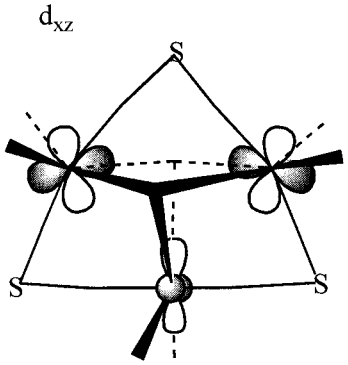

3

The vanadium−vanadium distance within the octahedron trimer is 3.162 Å, which is between the sums of the covalent radii (1.22 Å) and the atomic radii (1.92 Å). Therefore, there will be some weak interaction between the vanadium atoms. Because the octahedra share faces, the strongest interaction will be between the orbitals pointing to the shared octahedron faces. These are the d_{xz} orbitals of the t_{2g} set in the local coordinate system. The bonding combination is shown in **3**. Because these orbitals avoid the ligand direction, they are of ligand−metal nonbonding character. Furthermore, through the bonding interaction in **3**, they are at the bottom of the d band and contribute to metal−metal bonding within the octahedron trimer.

As described above, there are two octahedron trimers in the unit cell. They are joined together by sharing an octahedron edge. The distance between the two vanadium atoms at the centers of the two octahedra sharing the edge is the shortest metal−metal bond length at 2.8459 Å. When these two octahedron trimers are joined together, there will be bonding and antibonding combinations of the orbital shown in **3**. In fact the edge-sharing propagation of the trimer is through all three sides of the triangle in **3**, with one of the sides inside the unit cell and the other two at adjacent cells. The bonding combination is at the bottom of the d band illustrated in **2**. Of the total nine t_{2g} orbitals in the trimer, only one shown in **3** contributes to metal−metal bonding. Through the propagation of the trimers, only one-third of this orbital remains at the bottom of the d band. In other words, the maximum amount of doping per V_3S_4 trimer without filling the metal−metal or metal−ligand antibonding levels is about one-third of 2, or 0.6 electrons. Per V_6S_8 unit, the maximum doping is about 1.2 electrons.

Figure 7 shows the computed COOP curves of the metal−ligand and metal−metal bonds. The COOP curves represent the DOS-weighted overlap population plotted along the energy scale.[24] They indicate whether a set of states in a given energy range contributes to the bonding or antibonding character of a chemical bond of interest. Below the Fermi level in Figure 7, all states contribute to metal−ligand bonding as well as metal−metal bonding for the reason discussed above. However, more doping will result in the filling of the metal−metal antibonding level and, consequently, in the instability of the structure. In fact, we have not succeeded at achieving a doping level of more than one electron ($Ba_{0.5}$) per V_6S_8 unit. Excess doping of Ba in our study led to the different structure $BaVS_3$. Bensch and co-workers also reported a maximum doping of $Tl_{0.8}V_6S_8$, where Tl is believed to be Tl^{1+}.[7]

Raman Spectra. The space group $P6_3/m$ (no. 176) corresponds to the point group C_{6h}^2 with possible site symmetries C_{3h} (2), C_{3i} (2), $2C_{3h}$ (2), $2C_3$ (4), C_i (6), C_s (6), and C_1 (12).[25] Group theoretical analysis shows that there are 13 Raman-active modes ($3A_g + 2E_{1g} + 4E_{2g}$) and 20 IR-active modes ($10A_u + 10E_{1u}$). The A_g and E_{1g} vibrations only become Raman-active if one of the polarizability components in the *z* direction is changed, whereas the E_{2g} vibrations only become active if one of the polarizability components in the *xy* plane is changed. The spectra were taken with the polarization of the excitation source at 0°, 45°, and 90° (Figure 8) relative to the *z* (or *c*) axis of the crystal. With the polarization

(25) Nakamoto, K. *Infrared and Raman Spectra of Inorganic and Coordination Compounds*, 5th ed.; Wiley: New York, 1997.

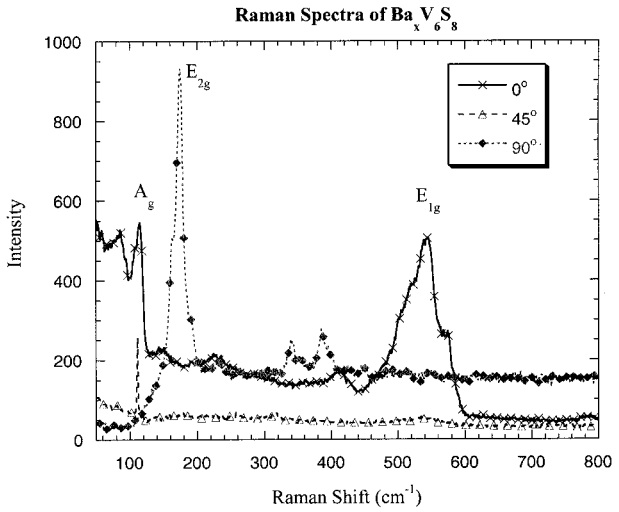

Figure 8. Raman spectra recorded with the polarization at 0°, 45°, and 90° relative to the *c* axis of the crystal.

of the excitation source parallel to the *z* axis, only the A_g and E_{1g} modes should be active because only the A_g and E_{1g} modes have a polarizability component active in the *z* direction. Therefore, all observed vibrations in this configuration should be attributed to the A_g and E_{1g} modes. As we rotate the crystal (from 0° to 45° to 90°), the polarization of the light source goes from parallel to perpendicular to the *z* axis. This change in the direction of the polarization results in the diminishment of the A_g peaks due to a weaker *z* component in the electric field vector of the excitation source and the development of the E_{2g} peaks due to a strengthening *xy* component. Figure 8 exhibit these trends. For example, the peak at 112 cm^{-1} is particularly strong and sharp at 0°. At 45°, this same peak is still observed, but a new minor peak at 174 cm^{-1} starts to appear. Finally, at 90°, the peak formerly observed at 112 cm^{-1} is completely absent, but the peak at 174 cm^{-1} is predominant. From this treatment, we can see that the peak at 112 cm^{-1} arises from the A_g mode and the peak at 174 cm^{-1} arises from the E_{2g} mode. Similarly, we can assign the peak at 545 cm^{-1} as the E_{1g} mode. Although no Raman data for other Ba−V−S compounds were available for comparison, computational results of the bond strengths led us to attribute the A_g and E_{2g} modes to S−V−S bending and E_{1g} to V−S stretching motions.

Superconductivity. Figure 9 shows the measured AC susceptibility of $Ba_xV_6S_8$. The filled circle is the real (in-phase) component, and the open circle the imaginary (out-of-phase) component of the volume susceptibility (SI units). The superconducting onset occurs at approximately 2.5 K. Superconductivity was not observed

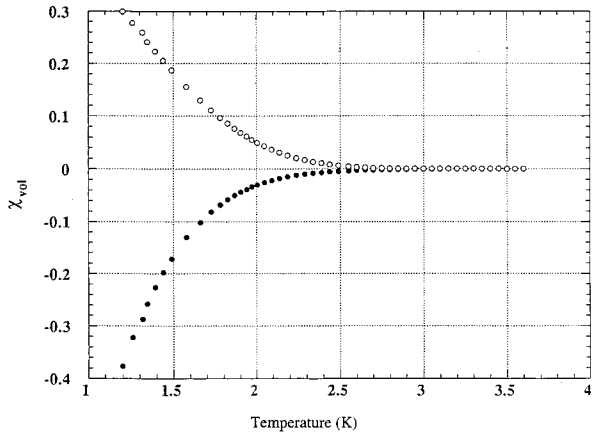

Figure 9. AC magnetic susceptibility of $Ba_xV_6S_8$. The open circle is the real part, and the dot is the imaginary part.

for the undoped sample V_6S_8 by us or by Bensch and co-workers.[7] It is interesting to note that the computed DOS (Figure 5) shows a maximum immediately above the Fermi level of $Ba_xV_6S_8$. The Fermi level of an undoped sample will be close to a minimum of the DOS at around −11.5 eV. Therefore, doping should increase the transition temperature according to the BCS theory. On the other hand, excess doping will increase the antibonding character in the structure so that the structure might no longer be thermodynamically stable. Thus, doping is allowed only in a particular range according to our computational analysis.

Conclusions

The group 5 transition metal ternary sulfide $Ba_xV_6S_8$ has been synthesized and analyzed. A superconductivity transition around 2.5 K was observed. Further study on the optimal doping of the title compound will be carried out in the future.

Acknowledgment. We thank the National Science Foundation for support of our research through Grants DMR-9704048 and CHE-9974760. Work at Argonne National Laboratory was performed under the auspices of the Office of Basic Energy Sciences, Division of Material Sciences, U.S. Department of Energy, Contract W-31-109-Eng-38. We also thank Robert L. Bailey of the Department of Geology at Northern Illinois University for assistance with the microprobe measurement.

Supporting Information Available: One X-ray crystallographic file is available (CIF). This material is available free of charge via the Internet at http://pubs.acs.org.

CM000396D